Pergamon

Int. J. Heat Mass Transfer. Vol. 41, No. 13, pp. 2003–2011, 1998

Printed in Great Britain
0017-9310/98 $19.00+0.00

PII: S0017-9310(97)00255-X

A numerical study of transient mixed convection in cylindrical thermal storage tanks

ROBERT E. SPALL†

Department of Mechanical and Aerospace Engineering, Utah State University, Logan, UT 84322-4130, U.S.A.

(*Received* 22 *April* 1997 *and in final form* 19 *August* 1997)

Abstract—The natural stratification of turbulent flows in an axisymmetric, cylindrical, chilled-water storage tank has been investigated numerically. The calculations involve the injection of cold water through a slot in the base of an insulated tank, within which the fluid is initially at rest and at constant temperature. Calculations are presented for inlet Reynolds numbers ranging from 500–3000, and Archimedes numbers ranging from 0.5–5.0. Results obtained by employing both k–ε and full Reynolds stress turbulence closure models are presented and contrasted, and indicate that to ensure stratified flow the Archimedes number should be greater than two, independent of the inlet Reynolds number. In addition, considerable differences were found in terms of the thickness of the evolving thermocline between the predictions of the k–ε and Reynolds stress models. © 1998 Elsevier Science Ltd. All rights reserved.

INTRODUCTION

Naturally stratified chilled water storage systems are utilized as a source of thermal energy to provide cooling for applications such as building cooling systems and gas turbine combustion inlet air (cf., Andrepont [1]). In the case of the gas turbine, refrigerative cooling techniques are employed to cool water at night, when electrical demand and costs are low. This stored water is then utilized during peak daytime hours to cool the turbine inlet air temperatures. The result is a significant boost in gas turbine outlet during peak summer demand. For building cooling systems, utility rate structures provide incentive for facilities to operate refrigeration equipment at night and store the thermal energy for later use during daytime hours when utility rates are higher. Equally important, daytime peaks of power consumption are reduced, thus delaying the need to build new power plants.

Along with this interest in demand side management must come advances in associated technologies such as chilled water thermal storage. The earliest relevant two-dimensional numerical work appears to be that of Chan *et al.* [2] in which the effects of inlet and outlet configurations on the transient temperature and velocity distributions for mixed convection flows in rectangular thermal storage tanks was studied. Guo and Wu [3] performed a similar study albeit for a storage tank containing two inlets and two outlets. Each of these studies considered laminar flows only. More recently, Ghajar and Zurigat [4] investigated the effect of inlet geometry on stratification within a cylindrical storage tank. They found negligible effect for Archimedes numbers greater than approximately 10. Additional numerical and experimental work concerning inlet design and its influence on mixing may be found in Zurigat *et al.* [5] and Abu-Hamdan *et al.* [6].

Cai and Stewart [7] developed a two-dimensional numerical model to predict turbulent mixing and thermal stratification for a side-slot tank inlet as a function of Reynolds number and Archimedes number. To ensure thermal stratification of the hot and cold water, they found that the Archimedes number should be greater than five, and the Reynolds number less than 1000.

Mo and Miyatake [8], somewhat critical of the numerical schemes utilized in some of the earlier studies, revisited the two-dimensional problem, performing interpolations in the discretization of the energy equation using both first-order upwinding, and a third-order QUICKEST (QUICK with estimated streaming terms) scheme [9]. A considerable decrease in the effects of numerical diffusion were noted when the QUICKEST scheme was implemented. (However, the convection terms in the remaining equations were treated using a first-order donor-cell method.) Cai and Stewart [7] and Mo and Miyatake [8] each employed a two-equation k–ε model for turbulence closure.

Most recently, Bouhdjar *et al.* [10] presented results for the transient mixed convection of laminar flows in a vertical cylindrical cavity. Somewhat contrary to the findings of Mo and Miyatake [8], Bouhdjar *et al.* indicate they were able to achieve grid converged solutions for relatively coarse grids using a first-order accurate power-law discretization scheme (albeit for laminar flows only).

In general, the mixing of the lower cold fluid and warmer upper fluid is inhibited due to the influence of

† E-mail: spall@fluids.me.usu.edu.

NOMENCLATURE

Ar	Archimedes number	U	velocity
g	acceleration due to gravity	x	axial coordinate.
h	inlet slot height		
H	height of storage tank	Greek symbols	
I	turbulence intensity	β	thermal expansion coefficient
k	turbulence kinetic energy	ε	turbulence dissipation rate
L	turbulence length scale	ρ	density.
r	radial coordinate		
R	radius of storage tank		
Re	Reynolds number	Subscripts	
t^*	time	0	signifies inlet properties
T	temperature	i	initial conditions.

buoyancy forces. At higher Reynolds numbers however, some investigators have reported that the enhanced mixing due to turbulence may decrease the degree of stratification. It is well known that turbulent mixing is strongly dependent upon the nature of the mean flow, which is itself highly dependent upon the geometry. As indicated above, most previous numerical studies have considered only rectangular shaped storage tanks, although in practice, cylindrical tanks are more commonly employed (cf., Dorgan and Elleson [11]). It is the primary intent of this work to perform a numerical study of the thermal stratification of turbulent flows within cylindrical storage tanks. Solutions obtained using both k–ε and differential Reynolds stress turbulence closure models will be presented and contrasted. In addition, a comparison of results computed using both power law (cf., Patankar [12]) and QUICK discretization schemes will be made (including an investigation of the consequences of employing QUICK discretization to only the energy equation).

MATHEMATICAL MODEL AND NUMERICAL METHOD

The governing equations consist of the incompressible Reynolds-averaged momentum, continuity, energy equations, and equations for turbulence closure, along with appropriate initial and boundary conditions. Two levels of turbulence modeling have been employed in this work: (1) the standard k–ε model based upon the Boussinesq hypothesis (cf., Launder and Spalding [13]), and (2) a differential Reynolds stress model (RSM). The pressure-based finite-volume code FLUENT (Fluent, Inc., Hanover, NH) was employed to solve the governing equations using cylindrical-polar velocity components.

The governing differential equations are well known, and hence for purposes of brevity they are not listed (cf., Hinze [14]). However, a brief description of the modeling assumptions employed in the RSM is appropriate. The diffusive transport term was represented by a simplified form of the generalized gradient diffusion hypothesis as:

$$-\frac{\partial}{\partial x_k}\left[\overline{(u_i'u_j'u_k')}+\frac{p}{\rho}(\delta_{kj}u_i'+\delta_{ik}u_j')-\nu\frac{\partial}{\partial x_k}\overline{(u_i'u_j')}\right] = \frac{\partial}{\partial x_k}\left(\frac{\nu_t}{\sigma_k}\frac{\partial}{\partial x_k}\overline{(u_i'u_j')}\right). \quad (1)$$

The pressure–strain term consisted of the linear return-to-isotropy and isotropization of production models for the 'turbulence' and mean-strain parts, respectively, as (cf., Launder *et al.* [15], Launder [16]):

$$\overline{\frac{p}{\rho}\left[\frac{\partial}{\partial x_j}u_i'+\frac{\partial}{\partial x_i}u_j'\right]} = -C_1\frac{\varepsilon}{k}\left[\overline{u_i'u_j'}-\frac{2}{3}\delta_{ij}k\right] - C_2\left[P_{ij}-\frac{2}{3}\delta_{ij}P-S_{ij}\right] \quad (2)$$

where the constants C_1 and C_2 were assigned the standard values of 1.8 and 0.60, respectively, and $P=\frac{1}{2}P_{ii}$. In addition, S_{ij} is a curvature related source term, arising from the cylindrical velocity formulation. In addition, P_{ij} is the production term, given as:

$$P_{ij} = -\overline{u_i'u_k'}\frac{\partial u_j}{\partial x_k}-\overline{u_j'u_k'}\frac{\partial u_i}{\partial x_k}. \quad (3)$$

The dissipation term was assumed isotropic, and was approximated by the scalar dissipation rate:

$$2\nu\overline{\frac{\partial}{\partial x_k}u_i'\frac{\partial}{\partial x_x}u_j'} = \frac{2}{3}\delta_{ij}\varepsilon \quad (4)$$

where the dissipation rate ε was computed via the ε transport equation. Finally, the relevant correlation in the energy equation was modeled using a gradient diffusion approximation.

Unless otherwise stated, interpolation to cell faces was performed using the QUICK (Leonard [9]) third-

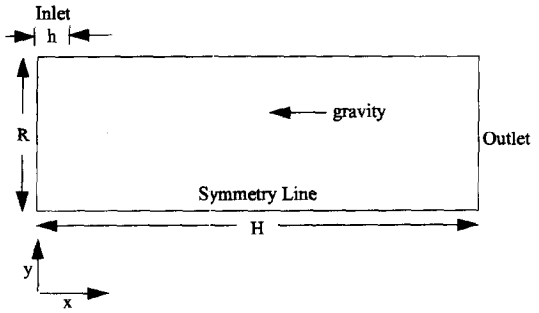

Fig. 1. Computational domain and coordinate system.

order interpolation scheme. First-order implicit differencing was employed for the temporal discretization and pressure–velocity coupling was based on the SIMPLE procedure (cf., Patankar [12]). Density variations were taken into account using the Boussinesq approximation for which density was treated as a constant value in all solved equations except for the buoyancy term in the momentum equations which was treated as:

$$(\rho-\rho_0)\boldsymbol{g} = -\rho_0\beta(T-T_0)\boldsymbol{g} \tag{5}$$

where ρ_0 and T_0 are the reference density and temperature, respectively, and β is the thermal expansion coefficient.

GEOMETRY AND PROBLEM FORMULATION

The baseline geometry consists of a cylindrical storage tank of radius R and depth H, containing an annulus of height h around the circumference of the tank base where the gravity vector is oriented in the negative x-direction (see Fig. 1). The importance of buoyancy forces in mixed convection flows is indicated by the ratio of the Grashof number to the square of the Reynolds number as $(\Delta\rho g h)/(\rho_0 U_0^2)$. In general, when this ratio exceeds unity, one may expect strong contributions from buoyancy. This ratio is also referred to as the Archimedes number (Ar), and when the density variation is accounted for by the Boussinesq approximation may be expressed as:

$$Ar = (\beta g h \Delta T)/U_0^2. \tag{6}$$

The relevant inlet Reynolds number for the problem is given as:

$$Re = (\rho_0 U_0 h)/\mu_0. \tag{7}$$

In the above dimensionless parameters, ρ_0 represents the reference density, μ_0 the reference viscosity, U_0 is a (uniform) inlet velocity, and $\Delta T = T_i - T_0$ (where T_0 is the inlet temperature).

At the jet inlet, the fluid properties were all assigned constant values. The magnitude of the turbulence kinetic energy (k) was derived from a fixed turbulence intensity (I) of 1% via the relationship $k = 1.5(U_0 I)^2$. Based upon scaling arguments, the dissipation rate was then given as $C_\mu^{0.75}k^{1.5}/L$, where $C_\mu = 0.09$ and the turbulence length scale L was taken as $0.07h$. In the case of the Reynolds stress model, the inlet shear stresses were set to zero, and the normal stresses to $2k/3$ (isotropic turbulence assumption). Symmetry conditions were imposed along the cylinder centerline, $r = 0$, while zero gradient conditions were imposed at the outlet boundary defined at $x = H$, where $H = 3R$. The intent was to develop an outlet boundary that would have minimum impact on the stratification properties of the flow. This implies that a significant region of one-dimensional flow should exist between the stratification zone and the outlet. Wall boundary conditions for the mean velocity, temperature (adiabatic wall), k, and ε were implemented using standard equilibrium wall functions.

At time $t = 0$, the fluid in the tank was assumed quiescent, at a constant temperature $T_i > T_0$. The turbulence kinetic energy was initialized to a negligibly small value, $k = 10^{-6}U_0^2$. Correspondingly, the initial condition for the dissipation rate was set to $\varepsilon = (C_\mu^{0.75}k^{1.5}/L)$.

A characteristic time was defined as

$$t^* = RH/(2U_0 h) \tag{8}$$

which represents the time necessary to fully replace the water in the tank when a plug flow occurs. The transient calculations were carried out over a time span $0.2t^*$, which was sufficient to determine the stratification properties of the flow. The time steps were chosen such that 500 time steps were required to reach the time level $0.2t^*$ (resulting in a dimensionless time step of 0.0004). Approximately 30 iterations per time step were required to drive the residuals to sufficiently low levels. In order to ensure that the time step was sufficiently small to accurately model the thermal and fluid transients, calculations at one half the above determined time step were also carried out.

The domain was discretized using 160 cells in the x-direction and 100 cells in the radial direction. The cells were clustered toward the lower wall (at $x = 0$) so that approximately 90 cells were contained over $0 \leqslant x \leqslant 0.9R$ (which bounds the inlet-to-stratification region over the time spans investigated). Cells were also clustered toward the symmetry plane and outer wall regions. Additional calculations were performed on a refined (320×200) grid to assess the grid convergence of the solution.

RESULTS

For the results to be presented, Archimedes numbers ranged from 0.5–5.0, and Reynolds numbers from 500–3000. In all cases, the Prandtl number was fixed at 12. These values are representative of what may be encountered in laboratory scale chilled water storage applications. Unless otherwise noted, the results to be presented were computed on the

160×100 grid with a dimensionless time step of $\Delta t = 0.0004$, using the Reynolds stress turbulence model, for the ratio $h/R = 0.1$. In addition, unless otherwise noted, results are presented at an inlet Reynolds number of 1000. Additional results will be presented to contrast Reynolds stress and k–ε model predictions. Calculations will also be presented to demonstrate the suitability of the aforementioned time step and grid resolution, and to investigate the effects of inlet Reynolds number and aspect ratio h/R on the stratification properties. Note that the figures to follow are oriented such that the fluid enters the domain at radius $r = R$, over the axial range $0 < x < 0.1R$.

Shown in Figs. 2(a)–(d) are contours of constant dimensionless temperature for $Ar = 0.5$, 1.0, 2.0, 5.0, respectively. The 15 evenly spaced contours range in value from 0–1.0. Contours are shown over the axial range $0 \leqslant x \leqslant 1R$, although the computational domain extends to $x = 3R$. The results indicate that for $Ar \leqslant 1.0$, mixing occurs between the warm and cold fluid, with a layer of relatively warm fluid developing along the bottom ($x = 0$) of the tank. Although not shown, the calculations at $Ar = 0.5$ and 1.0 were carried out for an additional 300 time steps, which resulted in continued mixing of the warm and cold fluids. In contrast to these lower Ar cases, at $Ar = 5.0$, the fluid has completely stratified, with a stratification thickness of approximately $0.35R$ (or $3.5h$). (The evolution of the $Ar = 0.5$ case for time levels below $0.2t^*$ is discussed at a later point.)

The effects of time step and grid resolution are assessed in Figs. 3(a)–(d). The results shown in Fig. 3(a) indicate temperature contours at $Ar = 1.0$ in which the grid employed was identical to that of Fig. 2(b); however the time step was reduced by a factor of two. Similarly, in Fig. 3(b) the time step of Fig. 2(b) was employed, however the number of grid points in each direction was doubled (320×200 grid). Similar comments apply to the results presented in Figs. 3(c) and (d) which represent calculations at $Ar = 5.0$. A comparison of the results shown in Figs. 2(b) and (d) (for $Ar = 1.0$ and 5.0, respectively) and 3(a) and (c) indicate that the time step $\Delta t = 0.0004$ is adequate; halving the interval resulted in only minor changes in the flowfield at $t = 0.2t^*$. In the case of grid refinement, qualitative differences exist for the $Ar = 1.0$ case shown in Fig. 2(b) (160×100 grid) and in Fig. 3(b) (320×200 grid), primarily along the $r = 0$ symmetry line. At $Ar = 5.0$, comparison of Figs. 2(d) and 3(d) reveals only a minor change in the temperature distribution. In each case, however, the conclusions drawn regarding the stratification of the flow remain unchanged, and hence, due to the large computer run times involved in computing 320×200 grid cases, the solutions obtained employing the 160×100 grid were deemed adequate for the purposes of this work.

Velocity vectors corresponding to the temperature contours of Figs. 2(a)–(d) are shown in Figs. 4(a)–(d). (For clarity, the vectors are plotted at every fourth grid point in both the axial and radial directions.) The results indicate the existence of an axial flow in the negative x-direction along the cylinder centerline that decreases in magnitude as Ar is increased from 0.5–

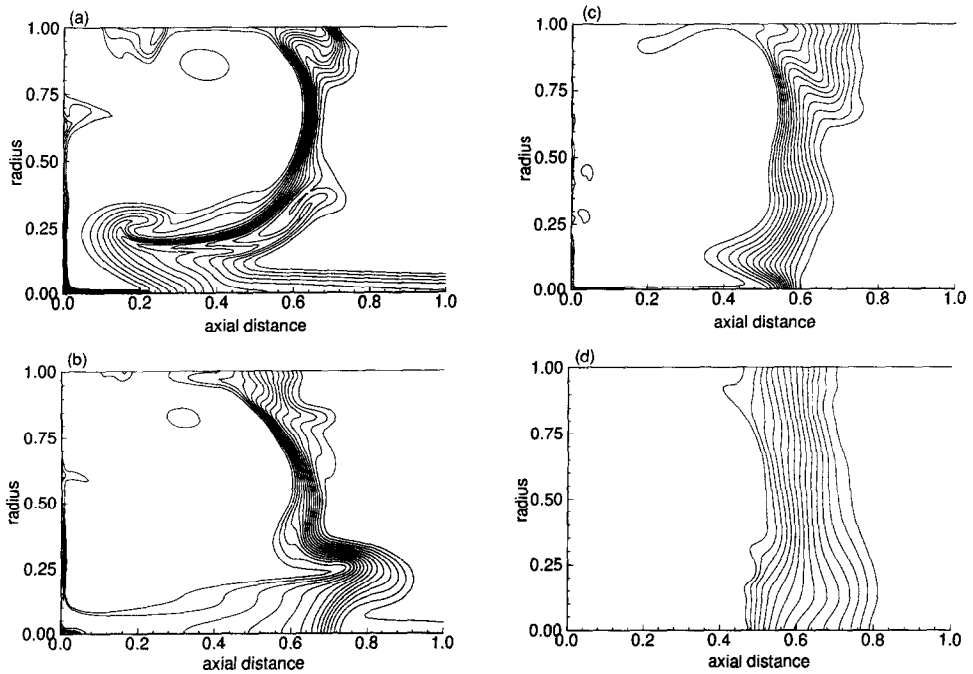

Fig. 2. Contours of constant temperature for $Re = 1000$. (a) $Ar = 0.5$; (b) $Ar = 1.0$; (c) $Ar = 2.0$; (d) $Ar = 5.0$.

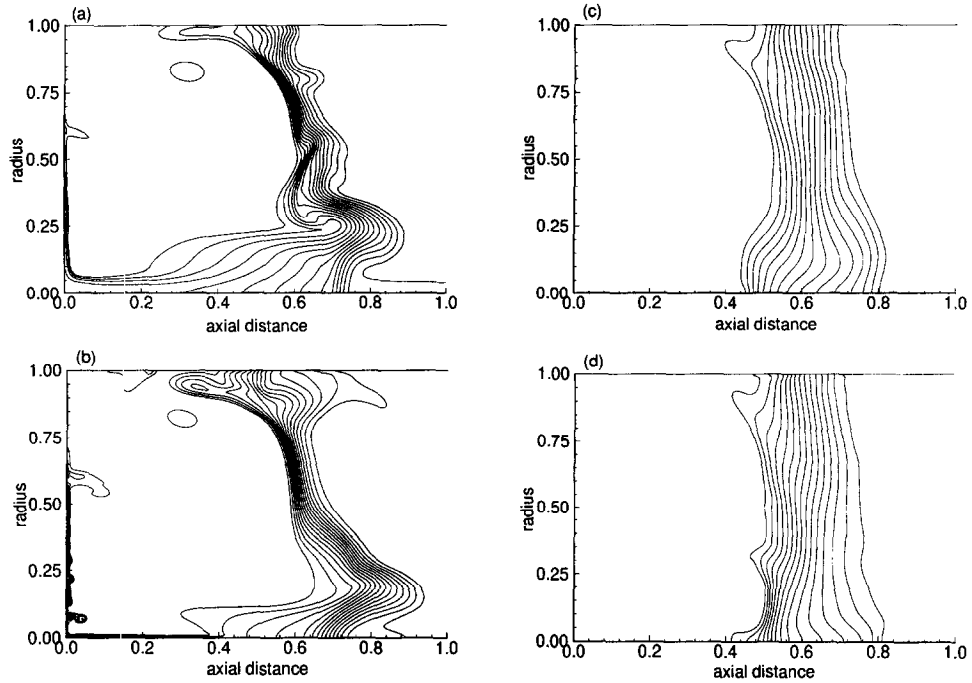

Fig. 3. Effect of increased grid resolution and decreased time step on contours of constant temperature. (a) $\Delta t = 0.0002$, $Ar = 1.0$; (b) 320×200 grid, $Ar = 1.0$; (c) $\Delta t = 0.0002$, $Ar = 5.0$; (d) 320×200 grid, $Ar = 5.0$.

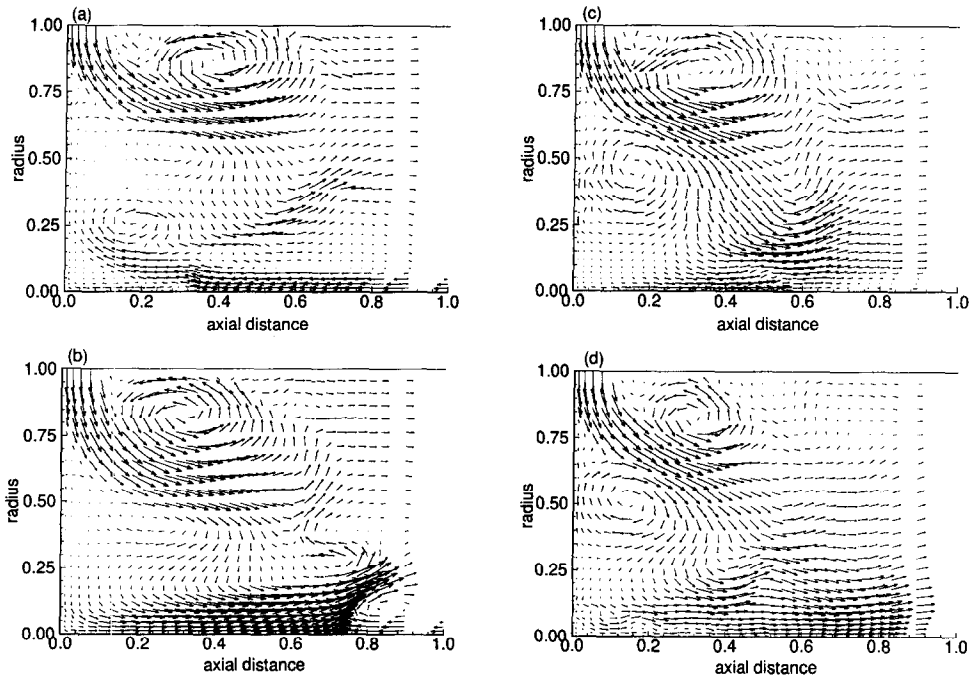

Fig. 4. Velocity vectors for $Re = 1000$. (a) $Ar = 0.5$; (b) $Ar = 1.0$; (c) $Ar = 2.0$; (d) $Ar = 5.0$.

2.0, and is completely absent at $Ar = 5.0$. The figures also reveal the existence of a pair of well-formed counter-rotating ring vortices near the inlet at $Ar = 2.0$ and 5.0. At lower values of Ar, the vortex nearer the outer tank wall exists; however, clear identification of the corresponding inner vortex is not possible. It is noted that in the complete absence of buoyancy effects, the only strong vortex to exist is that occurring near the outer wall—thus, the lower vortices occurring at $Ar = 2.0$, 5.0 are a direct consequence of buoyancy.

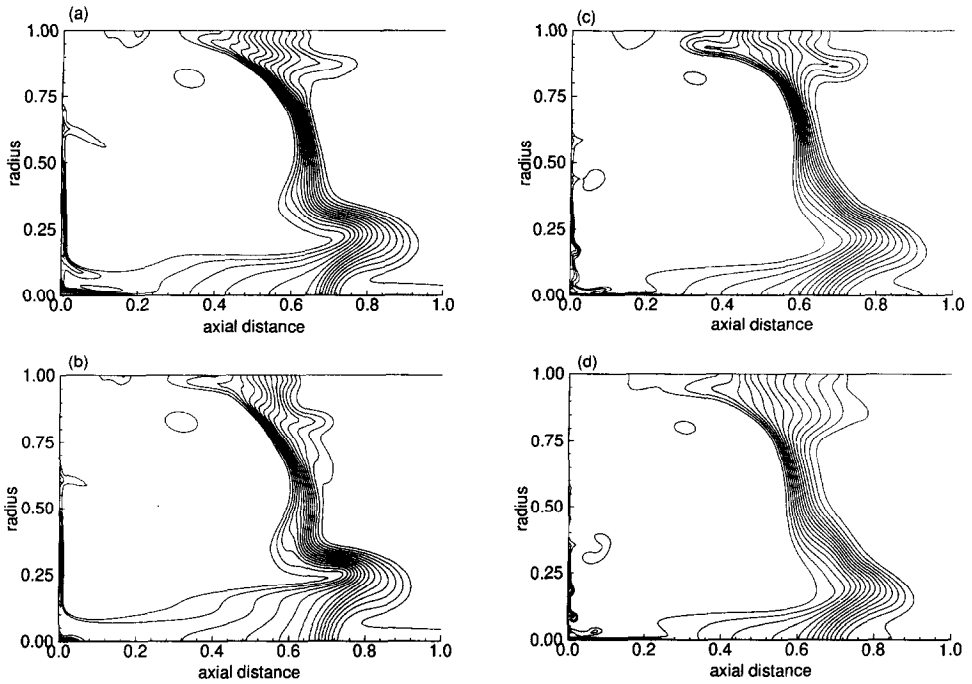

Fig. 5. Effect of Reynolds number on stratification properties at $Ar = 1.0$. (a) $Re = 500$; (b) $Re = 1000$; (c) $Re = 2000$; (d) $Re = 3000$.

To assess the effect of Reynolds number on the stratification properties of the flow, calculations were performed at $Ar = 1.0$ for Reynolds numbers 500, 1000, 2000 and 3000. Temperature contours for this set of calculations are shown in Figs. 5(a)–(d). The results indicate very little influence of Reynolds number on the stratification properties. In fact, the results actually reveal that as the Reynolds number is increased, a slight decrease in mixing occurs along the bottom of the tank. (This tendency can be explained by looking at the development of the flow at time levels below $0.2t^*$, as is done in the sequence of contours shown in Figs. 6(a)–(d), discussed in the next paragraph.) The Reynolds number independence at constant Ar is in accord with the results presented by Mo and Miyatake [8] for the transient motion of a stratified fluid in a two-dimensional rectangular storage tank, but contrary to the results of Cai and Stewart [7].

To gain some insight into the rather complicated flow pattern that developed for the $Ar = 0.5$, $Re = 1000$ case shown in Fig. 2(a), a series of temperature contours (for the same conditions) are presented at time levels $t = 0.04t^*$, $0.08t^*$, $0.12t^*$, $0.16t^*$ in Figs. 6(a)–(d). The contours reveal that at the initial stages, as a consequence of continuity, the inlet jet is lifted off the lower wall of the tank, trapping a portion of the initial warm fluid beneath the cooler inlet flow. However, at higher values of Ar, buoyancy forces tend to confine the fluid toward the tank bottom, decreasing the volume of warm fluid beneath the jet. The same general process governs the decrease in the levels of warm fluid along the lower wall observed as inlet Reynolds number was increased (Figs. 5(a)–(d)), albeit higher levels of radial momentum are responsible. At later time levels the flow patterns have resulted in the creation of a 'finger' of warm fluid extending well along the tank axis. At some point, the direction of the flow along the axis is reversed, and the warm fluid begins to descend toward the tank bottom. In terms of maintaining a thin and well defined stratification region, these low Ar flow patterns are clearly unacceptable. At $Ar = 2.0$, buoyancy forces are sufficiently large these patterns are essentially eliminated.

Shown in Figs. 7(a)–(d) are contours of constant temperature corresponding to the conditions in Figs. 2(a)–(d), respectively. However, the results in Fig. 7 were obtained by employing a standard k–ε turbulence closure model (cf., Launder and Spalding [13]), rather than the Reynolds stress model. The difference between the predictions of the two models is considerable. For each Ar number considered, the k–ε model predicted a thermocline on the order of 50–100% thicker than that predicted by the Reynolds stress model. In fact, for the intermediate levels of buoyancy ($Ar = 1.0$, 2.0), the qualitative features of the predictions are different. (Grid and time step refinement for the k–ε cases revealed no significant change in the results.) Although it is not suggested that the Reynolds stress model represent a standard of comparison, the overly diffusive nature of the k–ε model in many complex turbulent flows of industrial interest is well documented (cf., Nallasamy [17]). It is

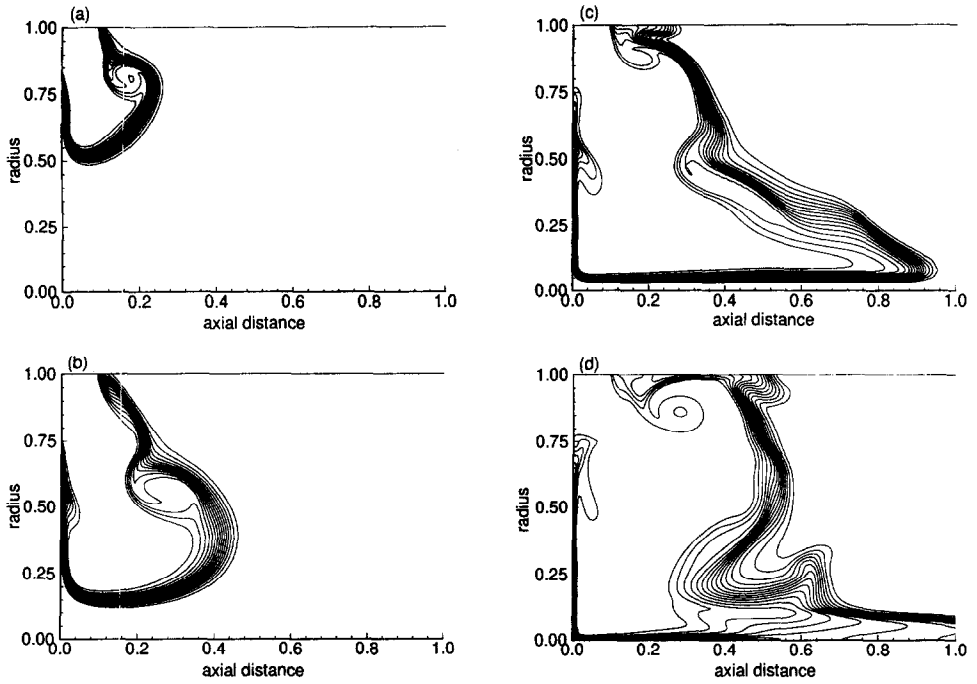

Fig. 6. Time accurate development of temperature field for $Ar = 0.5$, $Re = 1000$. (a) $t = 0.04t^*$; (b) $t = 0.08t^*$; (c) $t = 0.12t^*$; (d) $t = 0.16t^*$.

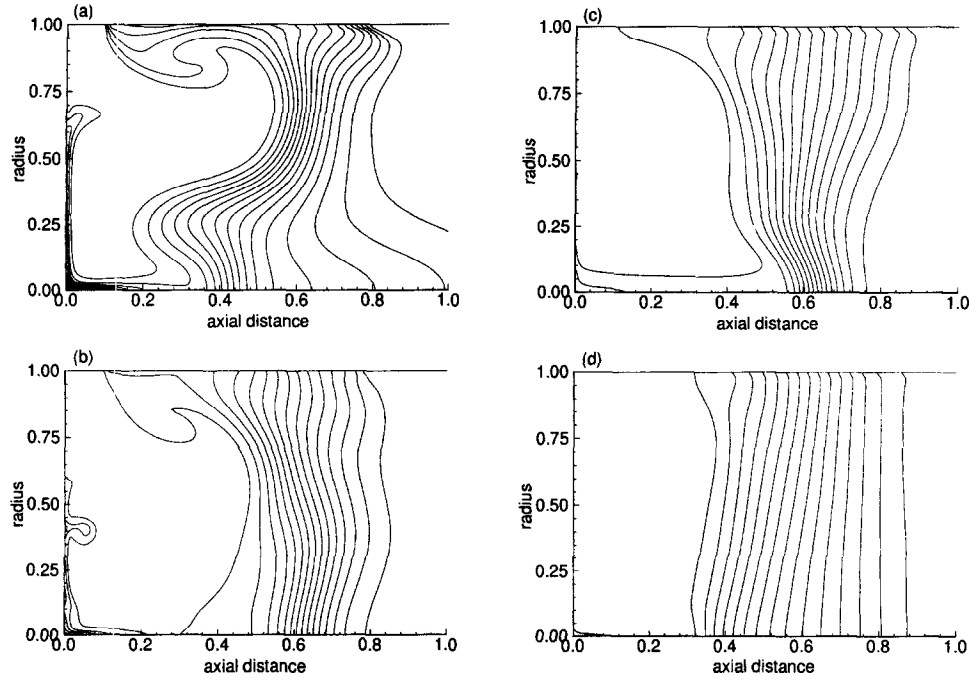

Fig. 7. Contours of constant temperature computed using the k–ε model for $Re = 1000$. (a) $Ar = 0.5$; (b) $Ar = 1.0$; (c) $Ar = 2.0$; (d) $Ar = 5.0$.

noted that modifications to (primarily) the ε transport equation have been introduced in the literature, however, the preferred approach is to employ Reynolds stress models, which inherently account for the effects of streamline curvature and body forces.

Based upon the results presented in Mo and

Miyatake [8], it was decided to investigate the effects of employing a first-order power law interpolation scheme to the entire system of governing equations, and as an additional calculation, to employ QUICK interpolation to the energy equation alone, with the power law scheme being applied to all others. (Recall from the Introduction that Mo and Miyatake found that by applying QUICKEST interpolation to the energy equation alone the thickness of the thermocline was considerably reduced.) The results of these calculations at $Ar = 5.0$, $Re = 1000$ are expressed in terms of temperature contours in Figs. 8(a) and (b). Figure 8(a) represents the case for which power law was applied to all equations, Fig. 8(b) the case in which QUICK was applied to the energy equation only. The results are consistent with the findings of Mo and Miyatake in that the thickness of the thermocline has been reduced when QUICK differencing is applied to the energy equation alone. However, a review of Fig. 2(d), which represents the calculations that employed QUICK differencing for all equations, is revealing. The results of those calculations are quite similar to the results obtained using the power law interpolation for all equations. The surprising result is that the combination of first-order power law and third-order QUICK interpolation schemes have produced a thermocline that is thinner than the (consistent) implementation of QUICK interpolation for all equations. Hence, it may be that the claims in Mo and Miyatake regarding the benefits of third-order interpolation on the energy equation only may be premature. Had they implemented a consistent third-order interpolation uniformly over all equations, their conclusions may have been different. (It should be remembered however, that a Reynolds stress model was implemented in the present calculations, whereas a two-equation k–ε model was employed in the work of Mo and Miyatake.)

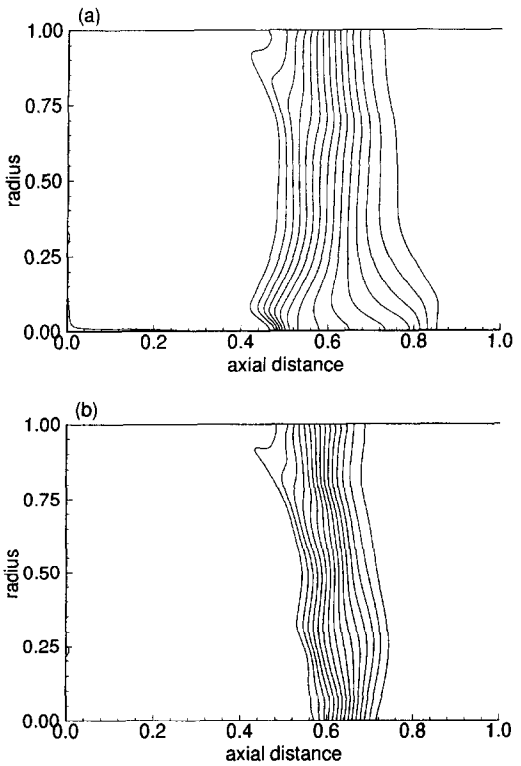

Fig. 8. Contours of constant temperature for $Ar = 5.0$, $Re = 1000$. (a) Interpolation using power law scheme for all equations. (b) Interpolation using QUICK scheme for energy equation and power law scheme for all others.

Finally, it is noted that a set of calculations similar to those leading to the results shown in Figs. 2(a)–(d) were also performed for a configuration with ratio $h/R = 2.0$. Qualitatively, the results mirrored those presented above, so the additional figures are not included. This result is consistent with discussions in Dorgan and Elleson [11].

CONCLUDING REMARKS

A numerical study of transient mixed convection in an axisymmetric cylindrical storage tank has been performed. In general, results published in the literature to date have indicated, where experimental data was available, that the numerical predictions overestimate the thickness of the thermocline. The present study has revealed that implementation of a Reynolds stress model rather than a two-equation k–ε model results in a considerable thinning of the thermocline. In addition, taken with the results of Mo and Miyatake [8], it appears that implementation of third-order interpolation for the energy equation only (with first-order interpolation in the remaining equations) may result in a reduction in thermocline thickness, when compared to consistent first-order or third-order interpolations for all equations. The interpretation of results obtained employing mixed accuracy interpolation, which in the work of Mo and Miyatake improved agreement with experiments, should be done with care.

The results also reveal that over the range investigated, inlet Reynolds number plays little role in determining the stratification properties of the fluid when the Archimedes number is held constant. This is consistent with the results of Mo and Miyatake [8] for the transient motion of a stratified fluid in a two-dimensional rectangular storage tank, but contrary to the results presented in Cai and Stewart [7].

Future work will concentrate on calculations for which the Boussinesq approximation is not employed, rather density will be specified as a non-linear function of temperature over the range of interest. This will coincide with an investigation of the stratification properties of water in the region near and below its density maximum (4°C).

Acknowledgement—The computational resources employed in this work were funded through a National Science

Foundation Academic Research Infrastructure grant (CTS-9632008).

REFERENCES

1. Andrepont, J. S., Performance and economics of CT inlet air cooling using chilled water storage. *ASHRAE Transactions*, 1994, **100**(1), 587–594.
2. Chan, A. M. C., Smereka, P. S. and Giusti, D., A numerical study of transient mixed convection flows in a thermal storage tank. *Journal of Solar Energy Engineering*, 1983, **105**, 246–253.
3. Guo, K. L. and Wu, S. T., Numerical study of flow and temperature stratifications in a liquid thermal storage tank. *Journal of Solar Energy Engineering*, 1985, **107**, 15–20.
4. Ghajar, A. J. and Zurigat, Y. H., Numerical study of the effect of inlet geometry on stratification in thermal energy storage. *Numerical Heat Transfer, A*, 1991, **19**, 65–83.
5. Zurigat, Y. H., Liche, P. R. and Ghajar, A. J., Influence of inlet geometry on mixing in thermocline thermal energy storage. *International Journal of Heat and Mass Transfer*, 1991, **34**, 115–125.
6. Abu-Hamdan, M. G., Zurigat, Y. H. and Ghajar, A. J., An experimental study of a stratified thermal storage under variable inlet temperature for different inlet designs. *International Journal of Heat and Mass Transfer*, 1992, **35**, 1927–1934.
7. Cai, L. and Stewart, W. E., Jr., Turbulent buoyant flows into a two dimensional storage tank. *International Journal of Heat and Mass Transfer*, 1993, **36**, 4247–4256.
8. Mo, Y. and Miyatake, O., Numerical analysis of the transient turbulent flow field in a thermally stratified thermal storage water tank. *Numerical Heat Transfer, A*, 1996, **30**, 649–667.
9. Leonard, B. P., A stable and accurate convective modelling procedure based on quadratic upstream interpolation. *Comput. Methods Appl. Mech. Eng.*, 1979, **19**, 59–98.
10. Bouhdjar, A. and Benkhelifa, A. Numerical study of transient mixed convection in a cylindrical cavity. *Numerical Heat Transfer, A*, 1997, **31**, 305–324.
11. Dorgan, C. E. and Elleson, J. S., *Design Guide for Cool Thermal Storage*. American Society of Heating, Refrigerating and Air-Conditioning Engineers, Atlanta, GA, 1992.
12. Patankar, S. V., *Numerical Heat Transfer and Fluid Flow*. Hemisphere Publishing Corp., Washington, DC, 1980.
13. Launder, B. E. and Spalding, D. B., *Mathematical Models of Turbulence*. Academic Press, 1972.
14. Hinze, J. O., *Turbulence*. McGraw-Hill, New York, NY, 1987.
15. Launder, B. E., Reece, G. J. and Rodi, W., Progress in the development of a Reynolds-stress turbulence closure. *Journal of Fluid Mechanics*, 1975, **68**, 537–566.
16. Launder, B. E., Second-moment closure: present... and future? *International Journal of Heat and Fluid Flow*, 1989, **10**, 282–300.
17. Nallasamy, M., Turbulence models and their applications to the prediction of internal flows: a review. *Computers and Fluids*, 1987, **15**, 151–194.